

Narrow (*n,m*)-Distribution of Single-Walled Carbon Nanotubes Grown Using a Solid Supported Catalyst

Sergei M. Bachilo,[‡] Leandro Balzano,[†] Jose E. Herrera,[†] Francisco Pompeo,[†]
Daniel E. Resasco,^{*†} and R. Bruce Weisman^{*‡}

School of Chemical Engineering and Materials Science, University of Oklahoma, 100 East Boyd Street, Norman, Oklahoma 73019, and Department of Chemistry, Center for Nanoscale Science and Technology, and Center for Biological and Environmental Nanotechnology, Rice University, 6100 Main Street, Houston, Texas 77005

Received June 11, 2003; E-mail: resasco@ou.edu; weisman@rice.edu

Because the electronic and optical properties of single-walled carbon nanotubes (SWNTs) depend sensitively on tube structure,¹ a major goal in SWNT production is to control the distribution of nanotube diameters and chiralities in the product. For methods in which nanotubes are grown from gaseous precursors on metallic catalyst particles, the size distribution of the catalyst particles strongly influences the product composition.² Dozens of distinct SWNT structures are formed in the HiPco process, in which disproportionation of CO into CO₂ and carbon nanotubes occurs on unsupported iron catalyst clusters formed in situ by the gas-phase decomposition of iron pentacarbonyl.³ A promising alternative CVD approach achieves high selectivities for SWNT formation using a silica-supported Co–Mo catalyst (CoMo CAT).⁴ It has been found that the product composition in this method depends on the Co:Mo ratio and on catalyst treatments that precede nanotube growth.⁵ In principle, adjustment of these parameters should allow fine control over the form of the active catalyst clusters and, therefore, of the nanotube structures. A major challenge in such process optimization has been assessing nanotube structure distributions formed under various conditions. However, recent breakthroughs in SWNT spectrofluorimetry provide a powerful new tool for such analyses.^{6,7} We report here results coupling the CoMoCAT preparation method with spectrofluorimetric analysis to reveal remarkably sharp product distributions of SWNT structures. We estimate that two specific structures, the (6,5) and (7,5) tubes, together comprise more than 50% of the semiconducting SWNT formed in this process.

The CoMoCAT synthesis was performed using a silica support (Sigma-Aldrich SiO₂ with 6 nm average pore size and BET surface area of 480 m² g⁻¹) and a bimetallic catalyst prepared from cobalt nitrate and ammonium heptamolybdate precursors. The total metallic loading in the catalyst was 2 wt %, with a Co:Mo molar ratio of 1:3. Before exposure to the CO feedstock, the catalyst was heated to 500 °C in a flow of gaseous H₂, and further heated to 750 °C in flowing He. The CO disproportionation reaction used to produce SWNTs was then run in a fluidized bed reactor under a flow of pure CO at 5 atm total pressure. The SWNTs grown by this method remained mixed with the spent catalyst, containing the silica support and the Co and Mo species. To eliminate the silica from this mixture, the solid product was suspended in a stirred 20% HF solution for 3 h at 25 °C. The suspension was then filtered through a PTFE 0.2 μm membrane and washed to neutral pH with deionized water. Next, the solid product was added to an aqueous solution containing the surfactant sodium dodecylbenzene sulfonate (NaDDBS) at twice its critical micelle concentration, and ultrasoni-

cally agitated for 1 h using a Fisher Scientific model 550 homogenizer (550 W output). This created a stable suspension of individual and bundled nanotubes. This suspension was centrifuged for 1 h at 72 600g to separate metallic catalyst particles and suspended tube bundles from the lower density surfactant-suspended individual nanotubes. Only a small fraction of the product deposited at the bottom of the centrifuge tube. Finally, the supernatant liquid, enriched in individual surfactant-suspended SWNTs, was withdrawn and adjusted to a pH between 8 and 9 for spectral analysis.

As was reported earlier, individual semiconducting SWNTs in suspension show characteristic wavelengths of visible absorption and near-infrared emission that have been assigned to specific nanotube structures.⁷ These structures can be labeled using (*n,m*) notation, in which integers *n* and *m* uniquely specify tube diameter and chirality.¹ To deduce the sample's (*n,m*) composition, we measured the intensity of light emission as a function of excitation and emission wavelengths using a J-Y Spex Fluorolog 3-211 spectrofluorometer with a liquid-N₂ cooled InGaAs detector. Excitation and emission spectral slit widths were 6 nm, and scan steps were 2–3 nm on both axes.

The raw data were corrected for wavelength-dependent instrumental factors and then graphed to give the contour plot in Figure 1 (top panel). The main intensity peaks are labeled with (*n,m*) indices assigned previously.⁷ Clearly, only a few structures dominate the semiconducting nanotube distribution in our sample. Comparison with the comparable data segment from a HiPco sample (Figure 1, bottom panel) shows that the CoMoCAT product contains a much narrower structure distribution. Table 1 lists relative fluorescence intensities (15% estimated accuracy) for all structures detected in the CoMoCAT sample and major ones in the HiPco sample. The CoMoCAT sample shows two dominant structures: (6,5) and (7,5). Together, these account for 57% of the semiconducting tubes (presuming that abundance is proportional to fluorescence intensity). If metallic nanotubes comprise 1/3 of the total, the (6,5) and (7,5) structures represent 38% of all SWNTs in the CoMoCAT sample.

Data in Table 1 show that the semiconducting tubes from the CoMoCAT run have an average diameter of 0.81 nm, significantly below the 0.93 nm average found for a HiPco sample.⁷ Despite its smaller average diameter, the CoMoCAT sample contains no spectral features from tubes smaller than (5,4), which is also detectable in HiPco samples. This finding suggests that the small-diameter edge of the diameter distribution may be defined by stabilities rather than by catalyst particle size. Raman data on similar CoMoCAT samples are qualitatively consistent with the fluorimetric findings.⁸

[†] University of Oklahoma.

[‡] Rice University.

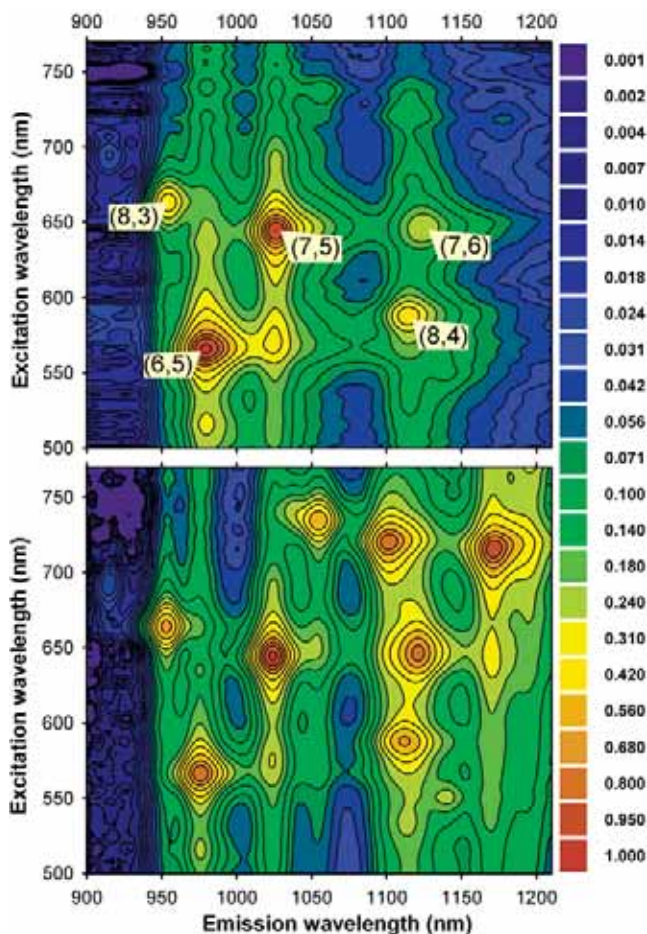


Figure 1. Contour plots of normalized fluorescence intensities for the CoMoCAT sample (top frame) and the HiPco sample (bottom frame).

Table 1. (n,m) -Resolved Spectral Intensities from SWNT Samples

n,m	diameter (nm)	chiral angle (deg)	fractional intensity (%), CoMoCAT	fractional intensity (%), HiPco
5,4	0.620	26.3	0.3	0.0
6,4	0.692	23.4	2.8	0.3
9,1	0.757	5.2	0.8	0.2
6,5	0.757	27.0	28	3.7
8,3	0.782	15.3	11	2.9
9,2	0.806	9.8	1.7	0.4
7,5	0.829	24.5	28	4.9
8,4	0.840	19.1	14	4.2
10,2	0.884	9.0	0.0	4.5
7,6	0.895	27.5	8.5	7.1
9,4	0.916	17.5	2.3	7.6
10,3	0.936	12.7	0.0	4.3
8,6	0.966	25.3	0.8	8.3
9,5	0.976	20.6	0.3	5.7
9,5	0.976	20.6	0.0	5.7
12,1	0.995	4.0	0.0	3.8
11,3	1.014	11.7	0.0	4.6
8,7	1.032	27.8	0.3	5.6
10,5	1.050	19.1	0.0	4.6

Figure 2 shows a graphene sheet map of possible nanotube structures, with (n,m) values labeling semiconducting species. The thickness of each hexagonal cell border is proportional to the observed spectral intensity for the enclosed (n,m) structure. This map clearly reveals that the intensity distribution is sharp not only in tube diameter, which is proportional here to a cell's distance from (0,0), but also in tube chiral angle, which ranges from 0° along the zigzag line to 30° along the armchair line. The data show a

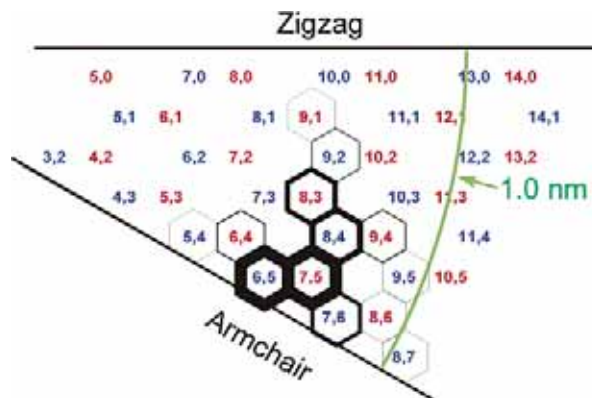


Figure 2. (n,m) -Resolved intensity map for the CoMoCAT sample. The thickness of each hexagonal cell in the graphene sheet is proportional to the observed intensity for that structure. Red and blue labels code for mod $(n-m,3)$ families, and the arc indicates tube diameters of 1.0 nm.

significantly stronger preference for near-armchair structures than was observed earlier in HiPco samples.⁷ For example, although the (9,1) and (6,5) tubes have the same diameter, the latter, with a chiral angle of 27° , shows 35 times the intensity of the former, which has a chiral angle of 5.2° .

We suggest that, in the CoMoCAT method, interactions between Mo oxides and Co stabilize the Co catalyst against aggregation through high-temperature sintering.⁵ We have found that these interactions vary with the Co:Mo ratio and evolve during stages of the catalyst life.⁹ At the low ratios used here, catalyst particles contain highly dispersed molybdenum oxide covered by a Co molybdate layer. With exposure to CO, the Mo oxide is converted into Mo carbide. This disrupts the molybdate layer, allowing the Co to be reduced by CO and migrate on the surface to form small, growing catalytic clusters of metallic Co. Carbon accumulates on these nanoclusters through CO disproportionation, leading to the formation of correspondingly small diameter SWNTs. The relatively low reactor temperature prevents the catalytic clusters from growing rapidly, which, as previously shown, would increase the average nanotube diameter.¹⁰ The growth mechanism also seems to strongly favor near-armchair structures. Further mechanistic studies using (n,m) product analysis are in progress.

Acknowledgment. This research was supported by the NSF (grants CHE-9900417, CHE-0314270, and CBEN center grant EEC-0118007), the Welch Foundation (grant C-0807), and the DOE (grant DE-FG03-02ER15345). We thank the Rice Carbon Nanotechnology Laboratory for a HiPco sample.

References

- (1) Saito, R.; Dresselhaus, G.; Dresselhaus, M. S. *Physical Properties of Carbon Nanotubes*; Imperial College Press: London, 1998.
- (2) Dai, H.; Rinzler, A. G.; Nikolaev, P.; Thess, A.; Colbert, D. T.; Smalley, R. E. *Chem. Phys. Lett.* **1996**, *260*, 471–475.
- (3) Nikolaev, P.; Bronikowski, M. J.; Bradley, R. K.; Rohmund, F.; Colbert, D. T.; Smith, K. A.; Smalley, R. E. *Chem. Phys. Lett.* **1999**, *313*, 91–97.
- (4) Kitiyanan, B.; Alvarez, W. E.; Harwell, J. H.; Resasco, D. E. *Chem. Phys. Lett.* **2000**, *317*, 497–503.
- (5) Herrera, J. E.; Balzano, L.; Borgna, A.; Alvarez, W. E.; Resasco, D. E. *J. Catal.* **2001**, *204*, 129–145.
- (6) O'Connell, M.; Bachilo, S. M.; Huffman, C. B.; Moore, V.; Strano, M. S.; Haroz, E.; Rialon, K.; Boul, P. J.; Noon, W. H.; Kittrell, C.; Ma, J.; Hauge, R. H.; Weisman, R. B.; Smalley, R. E. *Science* **2002**, *297*, 593–596.
- (7) Bachilo, S. M.; Strano, M. S.; Kittrell, C.; Hauge, R. H.; Smalley, R. E.; Weisman, R. B. *Science* **2002**, *298*, 2361–2366.
- (8) Herrera, J. E.; Balzano, L.; Pompeo, F.; Resasco, D. E. *J. Nanosci. Nanotechnol.* **2003**, *3*, 1–6.
- (9) Alvarez, W. E.; Kitiyanan, B.; Borgna, A.; Resasco, D. E. *Carbon* **2001**, *39*, 547–558.
- (10) Alvarez, W. E.; Pompeo, F.; Herrera, J. E.; Balzano, L.; Resasco, D. E. *Chem. Mater.* **2002**, *14*, 1853–1858.

JA036622C